Anomalous Isosteric Enthalpy of Adsorption of Methane on Zeolite-Templated Carbon

Supporting Information

Nicholas P. Stadie*, Maxwell Murialdo, Channing C. Ahn, and Brent Fultz

W. M. Keck Laboratory, California Institute of Technology, 138-78, Pasadena, California 91125

*Corresponding author. E-mail address: nstadie@caltech.edu.

I. Introduction

Additional materials characterization and data analysis were performed to supplement the results reported in "Anomalous Isosteric Enthalpy of Adsorption of Methane on Zeolite-Templated Carbon." They are discussed here along with experimental details related to the results presented in the main article.

These additional results include cycling of methane adsorption in all three materials, verifying the full reversibility of methane uptake and exemplifying the precision between measurements. Relevant materials properties such as skeletal density, bulk density, and specific surface area are summarized. Elemental analysis experiments to determine the relative concentration of H in MSC-30 and ZTC-3 were performed, and the results are discussed in the context of the nature of the different skeletal density between the two materials.

The central result reported in this work is the increasing isosteric enthalpy of adsorption with increasing methane uptake in the zeolite-templated carbon, ZTC-3. This is an interesting deviation from expected behavior of high surface area carbon materials, that normally derive their properties from surface imperfections (edge terminations, defects, and surface roughness typically contribute to the extremely high surface area in carbons). There are numerous methods for determining the enthalpy of adsorption, and many common techniques lead to a perceived increase in enthalpy of adsorption even on materials for which an increase is unphysical. This is primarily because the interpolated data are subject to mathematical manipulation to calculate thermodynamic quantities of adsorption where small errors of the interpolated value lead to large deviations of the results. We have employed a robust procedure for calculating the absolute adsorption quantities from experimental data which does not require any empirical knowledge of material properties (such as total pore volume or surface area) and is essentially model-independent. In this way, the isosteric enthalpy of adsorption was determined as a function of pressure and temperature, even at uptake quantities beyond the maximum in Gibbs surface excess where traditional methods show well-documented errors.[1-3] Employing ideal-gas law assumptions or excess adsorption data instead of absolute both lead to incorrect interpretations of the isosteric thermodynamic quantities, and we present a thorough comparison of our methods to other methods to show that the increasing enthalpy of adsorption in ZTC-3 is a physical result and not an error of improper calculations.

We also include the complete set of raw experimental data as a resource for future studies of adsorption analysis methods.

II. **Materials Properties**

Maxsorb® MSC-30 superactivated carbon was obtained from Kansai Coke & Chemicals Company, Ltd. Activated carbon CNS-201 was obtained from A. C. Carbons Canada, Inc. All materials were degassed at 250°C under vacuum to < 0.1 mPa before use.

The details of material synthesis and principal materials properties of ZTC-3 were reported previously, along with the details of materials characterization methods (nitrogen adsorption isotherms, transmission electron microscopy, x-ray diffraction, etc.).[4] In summary, it was found that ZTC-3 has chemical properties similar to other ZTCs (being predominantly sp^2 hybridized carbon) and has very high template fidelity, having the structural traits of the best reported examples.[5, 6] Its hydrogen adsorption properties are among the highest of reported carbonaceous materials, but are proportional to surface area between 77-298 K as for other carbons. The narrow pore-size distribution centered at 1.2 nm is not optimized for hydrogen adsorption.

The materials properties relevant to the discussion of methane adsorption in this study are summarized in Table 1. The skeletal densities are the average over 10 helium pycnometry measurements per sample, performed between 0-3 MPa and 298 K. The approximate bulk densities were measured at room temperature by packing a 1 mL volumetric flask over multiple trials. BET surface areas are reported, as previously discussed.[4] The excess methane capacities measured at 247, 298, and ~523 K from Figure 2 are tabulated for comparison.

Table 1: Densities of, BET surface areas (SA) of, and excess uptake capacities of methane adsorption on CNS-201, MSC-30, and ZTC-3.

Material	Skeletal Density[◊] ($g\ mL^{-1}$)	Bulk Density[◊◊] ($g\ mL^{-1}$)	BET Surface Area ($m^2 g^{-1}$)	247 K CH_4 Capacity[†] ($mmol\ g^{-1}$)	298 K CH_4 Capacity[††] ($mmol\ g^{-1}$)	~523 K CH_4 Capacity[†††] ($mmol\ g^{-1}$)
CNS-201	2.1	0.50	1095 ± 8	7.45	5.98	2.48
MSC-30	2.1	0.27	3244 ± 28	20.2	14.5	5.16
ZTC-3	1.8	0.18	3591 ± 60	20.5	14.1	4.76

[◊] Skeletal density measured using He at 298 K between 0-3 MPa. [◊◊] Bulk density measured on maximum packing. [†] Measured at 247 K and Gibbs excess maximum pressure. [††] Measured at 298 K and Gibbs excess maximum pressure. [†††] Measured at 526, 521, and 518 K for CNS-201, MSC-30, and ZTC-3, respectively, at 10 MPa.

The skeletal density of ZTC-3, consistent with other ZTCs, is lower than the typical value expected for carbonaceous materials: 1.8 $g\ mL^{-1}$, 81% of the skeletal density of pure graphite. This can be explained by the significantly higher hydrogen content in ZTCs as determined by elemental analysis experiments. Elemental composition (CHN) of MSC-30 and ZTC-3 was determined by triplicate combustion experiments, using the Dumas method.[7] Samples were prepared by degassing at 250°C and sealed in foil packets in an argon glovebox with < 1 ppm H_2O, a critical step for obtaining an accurate estimate of the H content since any adsorbed H_2O would contribute to detected H. The results are summarized in Table 2. Average hydrogen content in ZTC-3 was 2.4 wt% H, approximately twice that in MSC-30: 1.2 wt% H. If

each atomic site where carbon is substituted for hydrogen retains its original skeletal volume, the difference in skeletal density would be 11%, a decrease from 2.1 to 1.9 g mL^{-1}. Additional decrease in skeletal density could be due to the presence of hanging C-H groups which have a larger atomic volume than a pair of sp^2 hybridized carbon atoms. This approximation gives a representative figure for the significance of increased H content to the skeletal density, an effect that is large enough to account for the difference between MSC-30 and ZTC-3.

Table 2: Elemental hydrogen concentration of MSC-30 and ZTC-3.

Material	H (wt%)	Average (wt%)
MSC-30	0.74	1.16
	1.32	
	1.42	
ZTC-3	2.78	2.44
	2.47	
	2.08	

III. DFT Pore-Size Comparison

Nitrogen adsorption/desorption isotherms were measured at 77 K, and pore-size distributions were calculated by the non-local density functional theory (NLDFT) method[8] using a carbon slit pore model and software provided by Micromeritics. A carbon cylindrical pore model was also analyzed, but did not fit the data as well as the slit pore model. The pore-size distributions in ZTC-3 and the commercial carbons are shown in Figure S1.

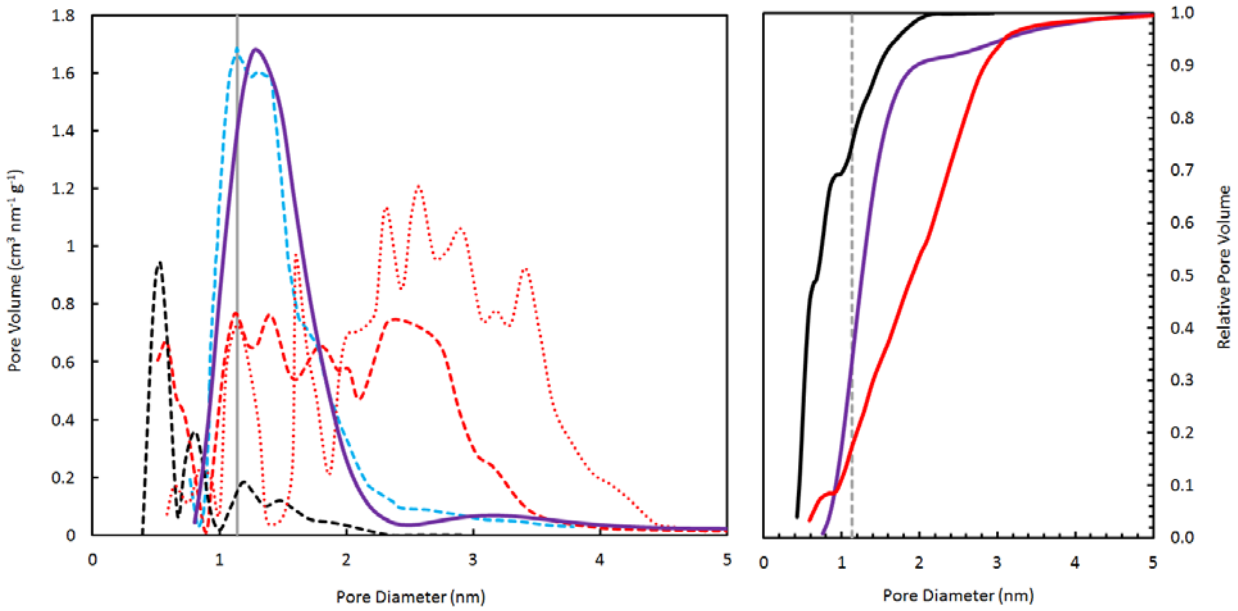

Figure S1. The pore-size distribution (left) and relative filling (right) of CNS-201 (black), MSC-30 (red), ZTC "P7(2)-H" (blue), and ZTC-3 (purple), calculated by the NLDFT method.[4, 5, 9, 10]

It has been proposed that 1.14 nm is the optimal spacing between graphene layers for maximum adsorption uptake of methane.[11, 12] The pore-size distribution of ZTC-3 has a mean pore-width close to this value, shown as a gray line in Figure S1. The relative pore volume as a function of pore-width is shown on the right, and ZTC-3 has the closest resemblance to an ideal step-function material with identical pores spaced at the optimal width.

IV. Methane Adsorption Measurements and Cycling

Methane adsorption isotherms at all temperatures were measured with a custom volumetric Sieverts apparatus, commissioned and verified for accurate measurements up to 10 MPa.[9, 13, 14] The apparatus was equipped with a digital cold cathode pressure sensor (I-MAG, Series 423), a high-resolution pressure manometer (MKS Baratron, Model 120AA), a high pressure manometer (MKS Baratron, Model 833), and a molecular drag pump to achieve a measurable pressure range of 10^{-5} to 10^{7} Pa. Temperature was measured on the wall of the manifold and on the outer wall of the sample holder using K-type thermocouples and platinum resistance thermometers (PRTs). The sample was submerged in a chiller bath for sub-ambient temperature isotherms. For high temperatures, the sample was placed inside a cylindrical copper heat exchanger and wrapped with insulated fiberglass heating tape. A PID controller and K-type thermocouples were used to maintain a consistent temperature throughout measurement; fluctuations were less than ±0.1 K at low temperature and no higher than ±0.4 K at high temperatures. The system was leak tested up to 10 MPa and showed a maximum leak rate of 7.0×10^{-6} mol h^{-1} of CH_4. If fitted to an exponential decay function, $n(t) = n_0 \exp(-kt)$ where k is the leak rate, this corresponds to a maximum leak of $k \sim 10^{-8}$ s^{-1} which is negligible for short time measurement.[15] The total inner volume of the apparatus was 66 mL.

Research purity methane (99.999%), obtained from Matheson Tri-Gas Inc., was exposed to the sample at incrementally higher pressures over the course of each isotherm in regular equilibration steps, allowing 10-30 min between gas expansions to ensure thermal equilibration. The system was not returned to vacuum in between steps and the measured uptake was cumulative from step to step. Cumulative uptake at each step was corrected for background adsorption of the instrument by subtracting the amount of perceived uptake at the same pressure in an empty sample holder. Empty sample holder "adsorption" was measured at each temperature, and was < 50% of total uptake (in grams) measured at all conditions in this study, a value beyond which the accuracy of measurements was assumed to be compromised. Gas densities were determined from temperature and pressure using the REFPROP Standard Reference Database.[16]

Prior to methane adsorption measurements, 0.3-1.5 g of sample was loaded and degassed at 250°C under vacuum to < 0.1 mPa for 12 h. Two adsorption runs were performed at each temperature and the combined data was tabulated for thermodynamic analysis. Complete adsorption/desorption cycles were also performed at various temperatures to assure full reversibility of methane physisorption in the complete temperature/pressure regime of study and to test the precision of the experiments. Error between cycles was < 1% of the measured value.

Adsorption/desorption cycling in all materials was achieved without any loss of capacity after many cycles, as expected for pure physisorbent materials. For example, three independent (non-consecutive) hydrogen adsorption/desorption cycles in ZTC-3 at 298 K are shown in Figure S2. The sample was degassed once before cycling but was not further treated between cycles. Equilibrium adsorption isotherms at 238, 298, and ~523 K are shown in Figure S3 for a direct comparison between the materials.

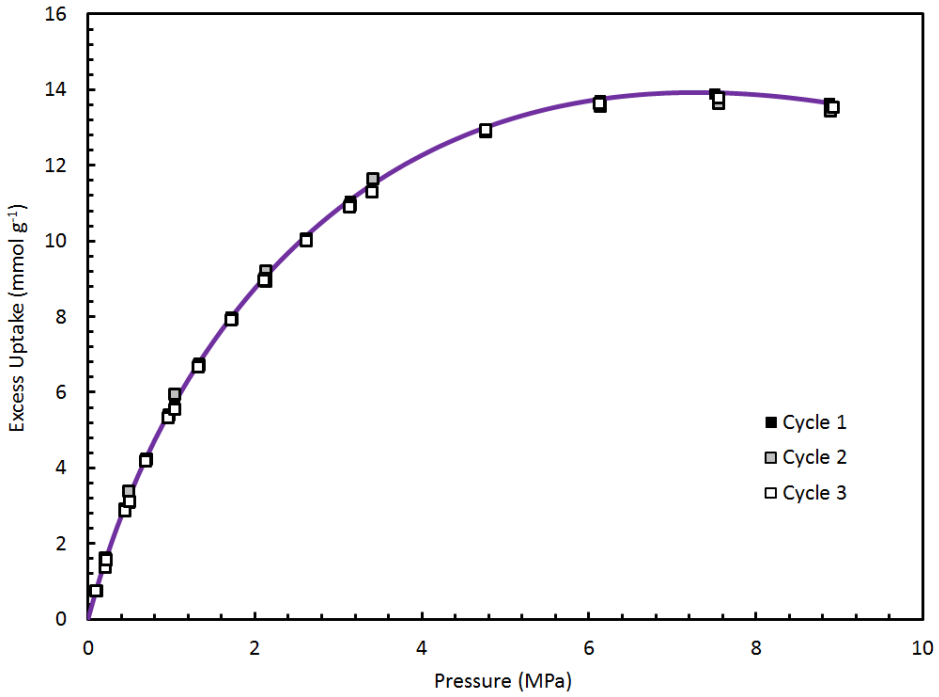

Figure S2. Equilibrium excess adsorption isotherms of methane on ZTC-3 at 298 K. Three cycles are shown, including adsorption and desorption points, displaying complete reversibility of uptake in these materials and showing typical precision between independent measurements.

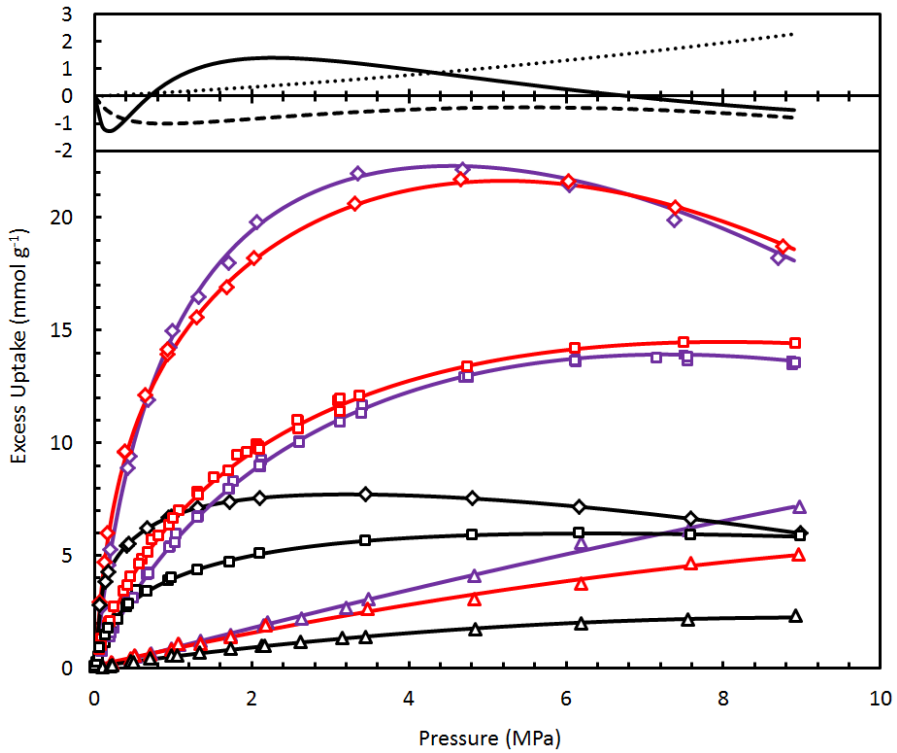

Figure S3. Comparison of equilibrium excess adsorption isotherms of methane on CNS-201 (black), MSC-30 (red), and ZTC-3 (purple) at 238 K (diamond), 298 K (square), and ~523 (triangle). The actual temperatures near 523 K are as given in Figure 2. The difference between ZTC-3 and MSC-30 is shown at the top: 238 K (full line), 298 K (dashed line), ~523 K (dotted line).

V. Isosteric and Isoexcess Equations of Adsorption

The following is a derivation of the thermodynamic quantities of interest for studies of high pressure methane adsorption. The change in entropy upon adsorption, ΔS_{ads} , can be calculated as a function of adsorption uptake, n_a, by the isosteric method (analogous to the Clausius-Clapeyron relation):

$$\left(\frac{dP}{dT}\right)_{n_a} = \frac{\left(s_a - s_g\right)}{\left(v_a - v_g\right)}$$

eq. 1

A typical assumption that accurately describes many experimental systems sets the change in molar volume as that of the gas phase change alone:

$$v_a - v_g \approx -v_g$$

eq. 2

Rather, we suggest a more accurate approximation:

$$v_a - v_g \approx v_{liq} - v_g$$

eq. 3

This becomes an important distinction at high pressure. Here, we use the molar volume of methane at 0.1 MPa and 111.5 K, v_{liq} = 38 mL mol^{-1}. Then:

$$\left(\frac{dP}{dT}\right)_{n_a} = \frac{\left(s_a - s_g\right)}{v_{liq} - v_g}$$

$$\Delta \mathrm{S}_{ads}(n_a) = \left(\frac{dP}{dT}\right)_{n_a} \left(v_{liq} - v_g\right)$$

eq. 4

$$\Delta \mathrm{H}_{ads}(n_a) = T\,\Delta \mathrm{S}_{ads} = T\left(\frac{dP}{dT}\right)_{n_a} \left(v_{liq} - v_g\right)$$

eq. 5

There are numerous approximations that can be used to simplify this expression. The most common is to assume the adsorbed molar volume is negligible relative to the gas. This gives:

$$\Delta \mathrm{H}_{ads}(n_a) = T\left(\frac{dP}{dT}\right)_{n_a} \left(-v_g\right) = -T\left(\frac{dP}{dT}\right)_{n_a} \left(\rho_g\right)^{-1}$$

eq. 6

In the ideal gas approximation (where we also keep the molar volume approximation):

$$\Delta \mathrm{H}_{ads}(n_a) = -T\left(\frac{dP}{dT}\right)_{n_a} \left(\frac{R\,T}{P}\right) = -\left(\frac{R\,T^2}{P}\right)\left(\frac{dP}{dT}\right)_{n_a}$$

eq. 7

This is commonly rearranged in the van't Hoff form:

$$\Delta \mathrm{H}_{ads}(n_a) = R\left(\frac{d\ln P}{d\left(\frac{1}{T}\right)}\right)_{n_a} \qquad \text{eq. 8}$$

The isosteric heat of adsorption is given a positive value (and it is common to report the "enthalpy" in this way as well), equal to -ΔH_{ads}. In summary:

Assumptions:	Isosteric Method	eq.	"Isoexcess" Method ($n_a \approx n_e$)	eq.
Ideal Gas $\Delta v_{ads} \approx -v_g$	$-\Delta \mathrm{H}_{ads}(n_a) = -\left(\frac{R\,T^2}{P}\right)\left(\frac{dP}{dT}\right)_{n_a}$	7	$-\Delta \mathrm{H}_{ads}(n_e) = -R\left(\frac{d\ln P}{d\left(\frac{1}{T}\right)}\right)_{n_e}$	9
Non-ideal Gas $\Delta v_{ads} \approx -v_g$	$-\Delta \mathrm{H}_{ads}(n_a) = T\left(\frac{dP}{dT}\right)_{n_a} {\rho_g}^{-1}$	6	$-\Delta \mathrm{H}_{ads}(n_e) = T\left(\frac{dP}{dT}\right)_{n_e} {\rho_g}^{-1}$	10
Non-ideal Gas $\Delta v_{ads} \approx v_{liq} - v_g$	$-\Delta \mathrm{H}_{ads}(n_a) = T\left(\frac{dP}{dT}\right)_{n_a} (v_g - v_{liq})$	5	$-\Delta \mathrm{H}_{ads}(n_e) = T\left(\frac{dP}{dT}\right)_{n_e} (v_g - v_{liq})$	11

Another relevant set of equations (Eq. 9-11) are given for the "isoexcess" approximation, where the measured (excess) quantity of adsorption is used in the place of the absolute quantity. The limitations of each approximation, and the results from their analysis, are discussed below. The results were sensitive not only to the equation used above, but also to the fitting technique for data interpolation.

VI. Thermodynamic Analysis of Adsorption Isotherm Data

Adsorption isotherms are measured at a set of fixed temperatures. The resulting data gives a relationship between the equilibrium pressure and the excess uptake amount, n_e, at each temperature, and can be used in Eq. 9-11 to calculate the isoexcess enthalpy of adsorption. However, the uptake amount is not fixed, and interpolation of the data is necessary to determine the equilibrium pressure at an arbitrary uptake amount. A number of different methods were compared to interpolate the data measured in this study:

1. No fitting, approximate isoexcess method
2. Linear interpolation, isoexcess method
3. Virial-type fitting equation, isoexcess method
4. Langmuir-type fitting equation, isoexcess method
5. Langmuir-type fitting equation, isosteric method

A comparison was performed for the data of methane adsorption on CNS-201, MSC-30, and ZTC-3 to determine the effects of each method on the results, and a detailed description is given elsewhere.[17] The data collected in this study is one of the largest sets available of methane adsorption on carbon. A summary of the results is given below, and a complete description of the method adopted in this study follows.

The interpolation of adsorption data in the high pressure limit is very sensitive to the method used, and small deviations from the true value cause significant errors in the thermodynamic calculations.[1, 2, 18] All methods give a visually good approximation to the experimental data at low pressure in this data set. The high pressure regime is where the methods differ significantly. The first distinction is made between using the excess adsorption data itself (the isoexcess approximation), and employing a model to determine the absolute adsorption. Using the excess adsorption quantity for thermodynamic calculations is an acceptable practice for studies of adsorption well below the critical point (low pressure and temperature) where excess and absolute adsorption quantities are approximately equal. However, at temperatures and pressures near the critical point and above, thermodynamic calculations from excess adsorption data lead to well-documented errors.[1, 2] The enthalpy of adsorption calculated in the high coverage regime often shows an unphysical steep increase that is associated with the use of the excess quantity. It is simple to show that if $n_e < n_a$, the slope of the excess isosteres in the van't Hoff plot will be more negative than that of the correct absolute isosteres (since the pressure necessary to achieve a given state of uptake will be underestimated), effecting an apparent increase in the calculated enthalpy of adsorption. Pitfalls such as these are either ignored, or the data beyond moderate quantities of surface coverage are discarded. In either case, the isosteric enthalpy is not accessible for high pressures, and quantities calculated using excess uptake data must be referred to as "isoexcess" quantities.[19] Within the context of the isoexcess approximation, the four methods listed above perform satisfactorily for determining the average Henry's law value of the enthalpy of adsorption, and can be used as a standard for comparing the Henry's law result from the isosteric method detailed below. The only method that successfully determines the isoexcess enthalpy of adsorption beyond the Gibbs surface maximum is that using a monotonically increasing fitting function in the context of the Gibbs definition of surface excess. We use a generalized Langmuir equation in this study, but other monotonically increasing fitting equations have also been employed with successful results.[2, 17, 18]

To understand the true thermodynamic quantities of adsorption from experimentally measured adsorption data, a model is necessary to determine the absolute adsorption amount as a function of pressure. The necessary variable that remains unknown is the volume of the adsorption layer and numerous methods have been suggested to estimate it. Typical methods include fixing the volume of adsorption as the total pore volume of the sorbent material,[1] using a volume proportional to the surface area (assuming fixed thickness),[20] or deriving the volume by assuming the adsorbed layer is at liquid density.[21] Some approaches are specific to graphite-like carbon materials, such as the Ono-Kondo model.[22, 23] The most general approach is to let the adsorption volume be an independent parameter of the fitting equation of choice. The generalized-Langmuir equation,[1] the Langmuir-Freundlich[2] equation, and the Unilan equation[18] have been shown to be suitable fitting equations for determining absolute adsorption from excess uptake isotherms since they are monotonically increasing and contain a relatively small number of fitting parameters to achieve a satisfactory fit to the experimental data. We adopted a generalized-Langmuir fitting equation, and found that two superimposed Langmuir equations are sufficient to fit the data for the materials in this study.

Generalized-Langmuir Model of Adsorption

The Gibbs definition of excess adsorption as a function of absolute adsorption, n_a , is:

$$n_e = n_a - V_{ads}\,\rho_g(P,T)$$

eq. 12

An effective strategy is to choose a functional form for n_a that is monotonically increasing with pressure, consistent with the physical nature of adsorption. The Langmuir isotherm is one example. If an arbitrary number of Langmuir isotherms are superpositioned, referred to as a generalized-Langmuir equation, the number of independent fitting parameters can be easily tuned to suit the data. In this method, absolute adsorption takes the form:

$$n_a(P,T) = n_{max}\sum_i \alpha_i \left(\frac{K_i\,P}{1+K_i\,P}\right)$$

$$\sum_i \alpha_i = 1$$

eq. 13

The parameter n_{max} is a scaling parameter, to convert the unitless quantity of adsorption to relevant units. The α_i are weights of the component Langmuir equations. The K_i are the equilibrium constants of adsorption in the classical Langmuir model. They are constant with pressure but have a dependence on temperature. An Arrhenius equation is a simple and accurate description, also a form arrived at by statistical methods,[24] to define the adsorption constants, K_i, as:

$$K_i = \frac{A_i}{\sqrt{T}}\,e^{\frac{E_i}{RT}}$$

eq. 14

The volume of the adsorbed layer in the Gibbs equation also has a pressure dependence that is fundamentally unknown, but which is generally accepted to be monotonically increasing in most systems. It too can be approximated by a generalized Langmuir equation, greatly simplifying the final fitting equation and keeping the number of fitting parameters low:

$$V_{ads}(P,T) = V_{max}\sum_i \alpha_i \left(\frac{K_i\,P}{1+K_i\,P}\right)$$

eq. 15

The parameter V_{max} is the volume of the adsorption layer at maximum adsorption occupancy. The excess adsorption data are then fitted to:

$$n_e(P,T) = n_{max}\sum_i \alpha_i \left(\frac{K_i\,P}{1+K_i\,P}\right) - \left(V_{max}\sum_i \alpha_i \left(\frac{K_i\,P}{1+K_i\,P}\right)\right)\rho(P,T)$$

$$n_e(P,T) = \left(n_{max} - V_{max}\,\rho(P,T)\right)\left(\sum_i \alpha_i \left(\frac{K_i\,P}{1+K_i\,P}\right)\right)$$

eq. 16

The total number of fitting parameters (n_{max}, V_{max}, α_i, A_i, and E_i) is 3i +1. If the ideal gas law applies to the pressure and temperature regime of interest, the equation simplifies:

$$n_e(P,T) = \left(n_{max} - V_{max}\,\frac{P}{RT}\right)\left(\sum_i \alpha_i \left(\frac{K_i\,P}{1+K_i\,P}\right)\right)$$

eq. 17

The experimental data of methane adsorption on MSC-30, fitted by a double-Langmuir isotherm (*i* = 2) with the ideal gas assumption, are shown in Figure S4. For all but the highest pressures (P > 6 MPa) at low temperatures, the data are well approximated by this method. The interpolation between points, even near or at the Gibbs excess maximum, is representative of the physical nature of the system, and the extrapolation to high pressures shows much improved behavior compared to that of a virial-type fitting equation. A limitation of the ideal gas assumption is that the excess uptake isotherms cannot cross at high pressure, the lowest temperature data decreasing proportionally with pressure. However, this is not consistent with experimental results where it frequently occurs that low temperature data falls significantly below higher temperature data at the same pressure. This is entirely due to non-ideal gas interactions from a nonlinear change in gas density, and can be accounted for by using the more general equation (Eq. 16).

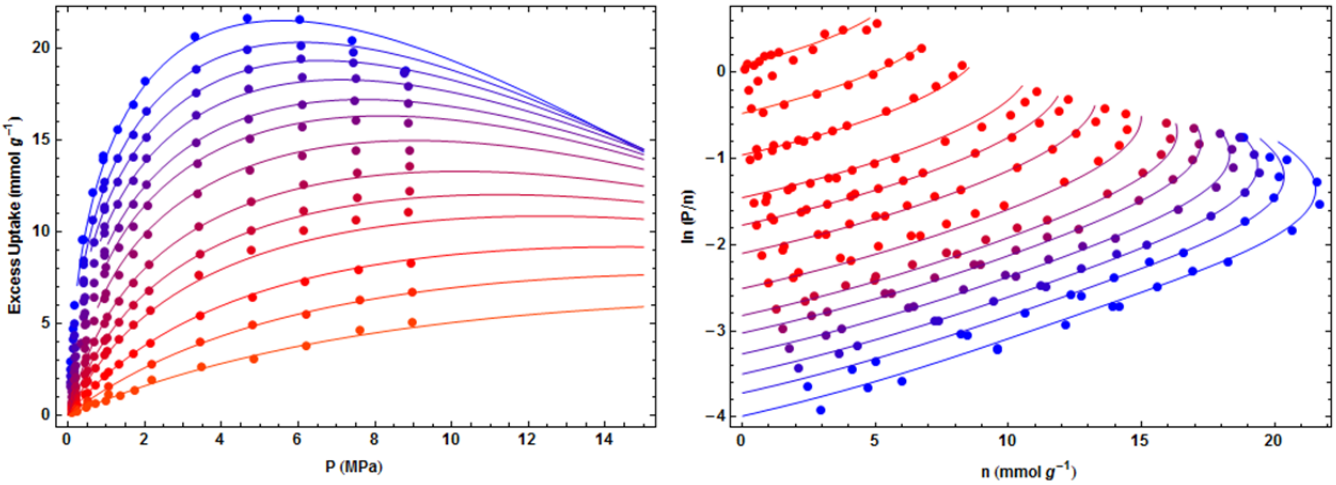

Figure S4. Double-Langmuir fit of the experimental data using the ideal gas law for the bulk gas phase.

The experimental data of methane adsorption on MSC-30 are shown in Figure S5, fitted using one, two, and three superimposed Langmuir isotherms (with 4, 7, and 10 independent parameters, respectively) and using the real gas density[16] for the bulk methane gas phase. A single Langmuir equation (*i* = 1) does not accurately fit the data. The double-Langmuir fit is visually satisfactory in the logarithmic plot of P/n_e, and is the preferred method in this study. The high pressure data are significantly better fitted by using the real gas density, and extrapolation of the low temperature data to pressures up to 15 MPa shows behavior consistent with that expected for excess adsorption at in these conditions. The triple-Langmuir fit is not a significant improvement, and cannot be justified for this data since a minimum number of independent parameters is desired. The reduced equation for *i* = 2 is:

$$n_e(P,T) = \left(n_{max} - V_{max}\,\rho(P,T)\right)\left((1-\alpha)\left(\frac{K_1\,P}{1+K_1\,P}\right) + \alpha\left(\frac{K_2\,P}{1+K_2\,P}\right)\right)$$

eq. 18

The assumption that the total adsorption volume scales proportionally with site occupancy is robust in this study, and this fitting equation has been previously shown to be successful for both carbonaceous and MOF materials.[1] We refer to this method (using *i* = 2) as the double-Langmuir method, and if the absolute quantity of adsorption is held constant, it yields the true isosteric quantities of adsorption. The absolute quantity, from the Gibbs definition, is:

$$n_a(P,T) = n_{max}\left((1-\alpha)\left(\frac{K_1 P}{1+K_1 P}\right) + \alpha\left(\frac{K_2 P}{1+K_2 P}\right)\right)$$

eq. 19

The fractional site occupancy, also called the surface coverage, is:

$$\theta(P,T) = (1-\alpha)\left(\frac{K_1 P}{1+K_1 P}\right) + \alpha\left(\frac{K_2 P}{1+K_2 P}\right)$$

eq. 20

Least squares fits of all of the experimental data (on CNS-201, MSC-30, and ZTC-3) to the double-Langmuir equation are shown in Figure S6, the fitted excess adsorption (left) and calculated absolute adsorption (right) at all temperatures measured. The goodness of fit was satisfactory across the entire range of temperature and pressure for all three samples, with a residual sum of squares less than 0.04 mmol g^{-1} per data point. The optimal fitting parameters for each material are given in Table 3.

Table 3: Least-squares minimized fit parameters of the double-Langmuir equation for methane adsorption on CNS-201, MSC-30, and ZTC-3 from equilibrium excess adsorption data measured between 238-526 K.

Material	n_{max} (mmol g^{-1})	V_{max} (mL g^{-1})	α	A_1 ($K^{1/2}$ MPa^{-1})	E_1 (kJ mol^{-1})	A_2 ($K^{1/2}$ MPa^{-1})	E_2 (kJ mol^{-1})
CNS-201	9.77	0.49	0.58	0.061	17.2	0.0044	16.4
MSC-30	41.0	2.30	0.70	0.068	13.4	0.0046	12.9
ZTC-3	35.6	2.04	0.46	0.059	11.6	0.00018	20.4

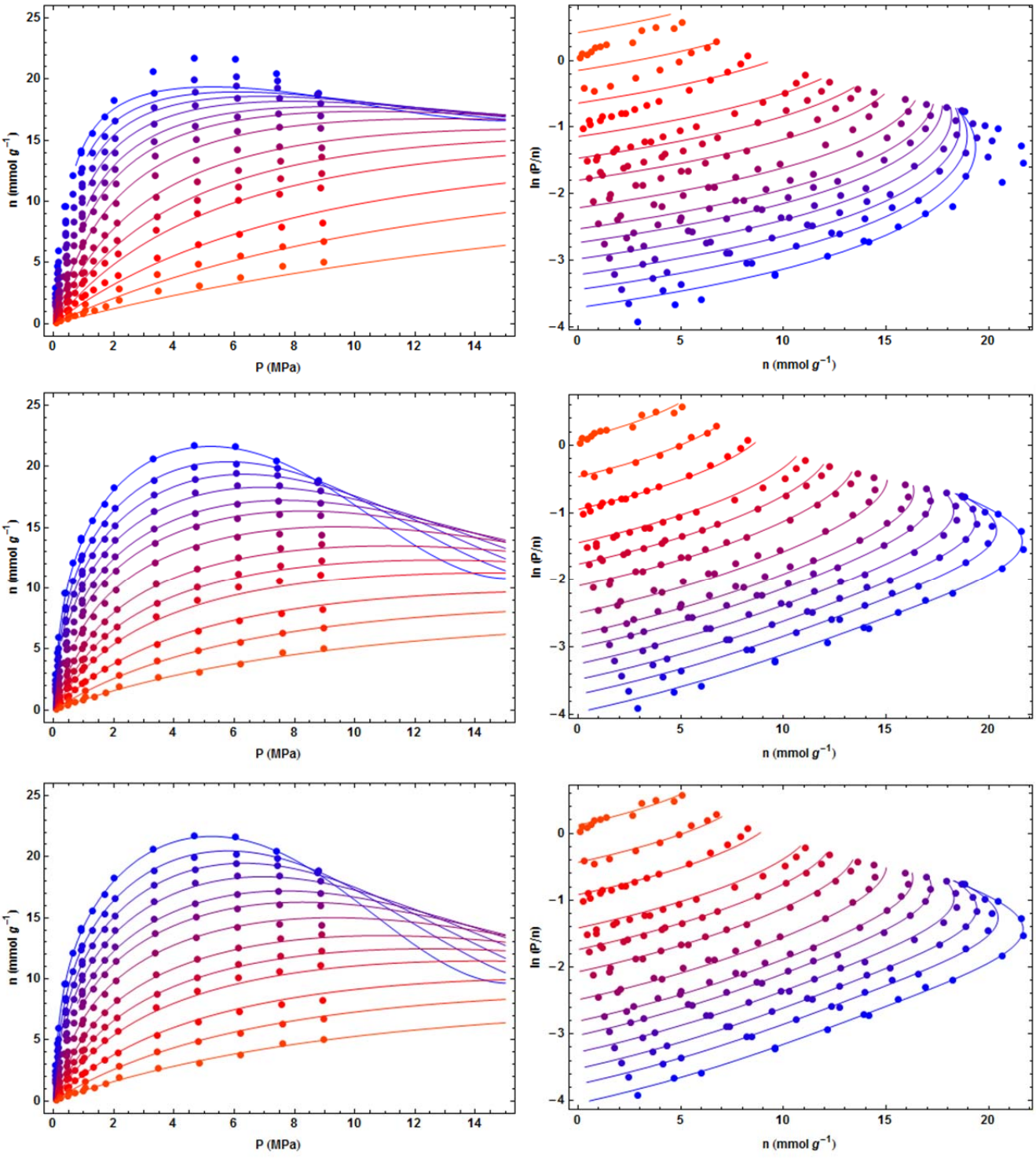

Figure S5. Single-, double-, and triple-Langmuir equation fits of the entire experimental data set.

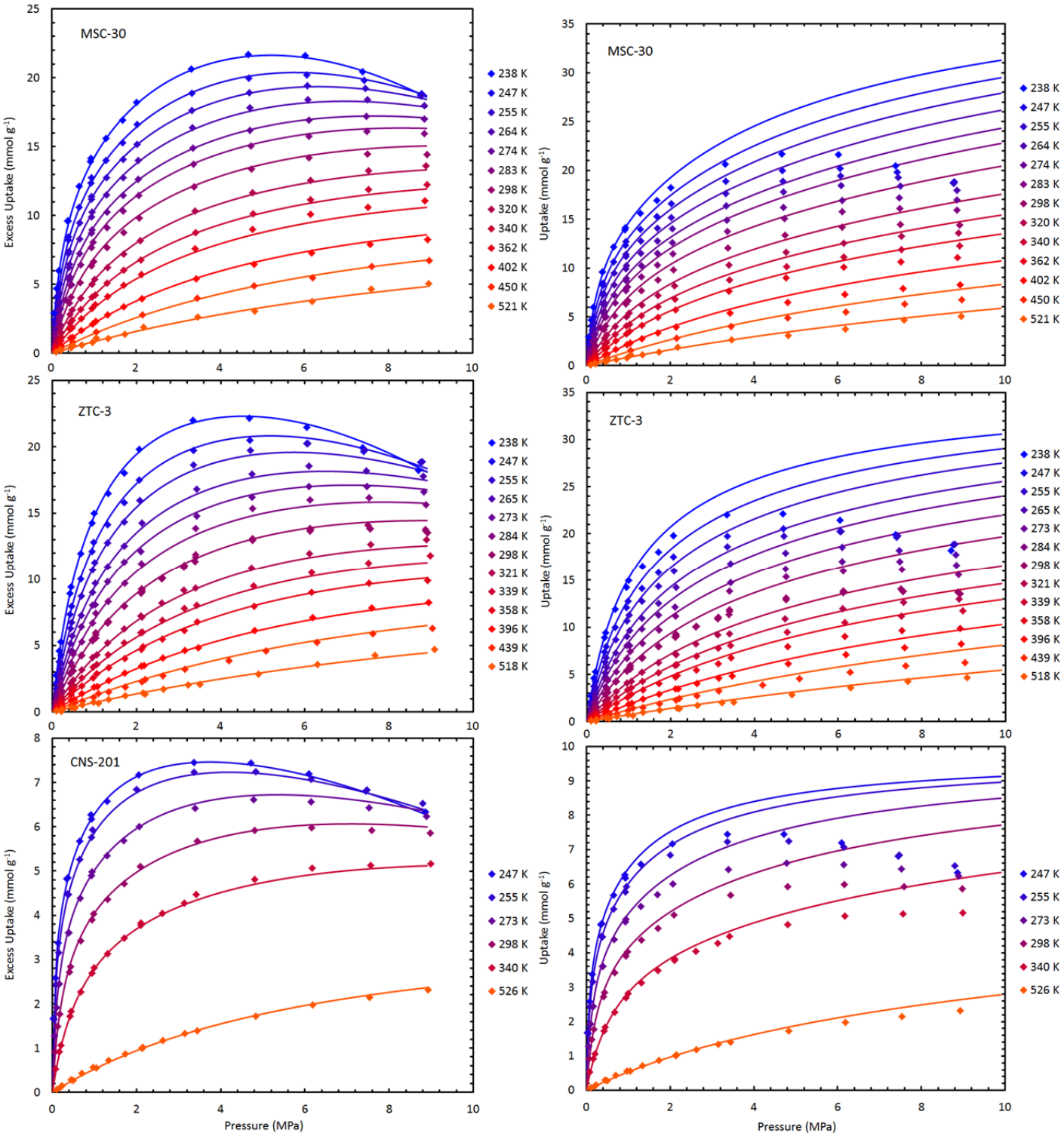

Figure S6. The complete set of experimental data, fitted to a double-Langmuir equation, of MSC-30 (top), ZTC-3 (middle), and CNS-201 (bottom): the fit results of excess uptake (left) and absolute uptake (right) at temperatures from 238-526 K (blue to orange). The diamonds are measured (excess) uptake.

To derive the isosteric enthalpy from the double-Langmuir equation, the derivative of pressure with respect to temperature is decomposed as follows:

$$\left(\frac{\partial \mathrm{P}}{\partial T}\right)_{\mathrm{n_a}} = \left(\frac{\partial \theta}{\partial P}\right)_{\mathrm{n_a}}^{-1} \left(\frac{\partial \theta}{\partial K}\right)_{\mathrm{n_a}} \sum_{\mathrm{i}} \left(\frac{\partial \mathrm{K_i}}{\partial T}\right)_{\mathrm{n_a}}$$

eq. 21

From Eq. 14 and 20, the respective components of the derivative are given by:

$$\left(\frac{\partial \theta}{\partial P}\right)_{\mathrm{n_a}} = \left(\frac{\partial}{\partial P}\right)_{\mathrm{n_a}} \left((1-\alpha)\left(\frac{K_1 P}{1+K_1 P}\right) + \alpha\left(\frac{K_2 P}{1+K_2 P}\right)\right)$$
$$= \left((1-\alpha)\left(\frac{K_1}{(1+K_1 P)^2}\right) + \alpha\left(\frac{K_2}{(1+K_2 P)^2}\right)\right) = X^{-1}$$

$$\left(\frac{\partial \theta}{\partial K}\right)_{\mathrm{n_a}} = \left(\frac{\partial}{\partial K}\right)_{\mathrm{n_a}} \left((1-\alpha)\left(\frac{K_1 P}{1+K_1 P}\right) + \alpha\left(\frac{K_2 P}{1+K_2 P}\right)\right)$$
$$= \left((1-\alpha)\left(\frac{P}{(1+K_1 P)^2}\right) + \alpha\left(\frac{P}{(1+K_2 P)^2}\right)\right) = \mathrm{Y}$$

$$\left(\frac{\partial \mathrm{K_i}}{\partial T}\right)_{\mathrm{n_a}} = \left(\frac{\partial}{\partial T}\right)_{\mathrm{n_a}} \left(\frac{A_i}{\sqrt{T}} e^{\frac{E_i}{RT}}\right) = -\frac{\frac{1}{2}RT + E_i}{RT^2} \frac{A_i}{\sqrt{T}} e^{\frac{E_i}{RT}}$$

$$\sum_{\mathrm{i}} \left(\frac{\partial \mathrm{K_i}}{\partial T}\right)_{\mathrm{n_a}} = -\frac{\frac{1}{2}RT + E_1}{RT^2} K_1 - \frac{\frac{1}{2}RT + E_2}{RT^2} K_2 = -Z$$

These are combined to arrive at the isosteric enthalpy of adsorption, in Eq. 5-7:

$$-\left(\frac{\partial \mathrm{P}}{\partial T}\right)_{\mathrm{n_a}} = \mathrm{X\,Y\,Z}$$

eq. 22

The isosteric enthalpy of adsorption of methane on MSC-30 is shown in Figure S7, using the most common approximations: the ideal gas law for the density in the gas phase, and the negligible molar volume of the adsorbed methane compared to the gas. The results are consistent with reported results for numerous sorbent systems and show a reasonable dependence of the isosteric enthalpy on both uptake and temperature. The Henry's law value is between 14.5-15.5 kJ mol^{-1}, consistent with the isoexcess results calculated without a fitting equation, and the enthalpy declines with uptake to 14 kJ mol^{-1}. Due to the ideal dependence of the gas density with pressure, the enthalpy reaches a plateau at high values of absolute uptake. This is a similar result as for hydrogen adsorption as well, since hydrogen is well approximated as an ideal gas in the typical ranges of temperature and pressure. However, methane is well known to deviate from ideality at conditions near ambient.

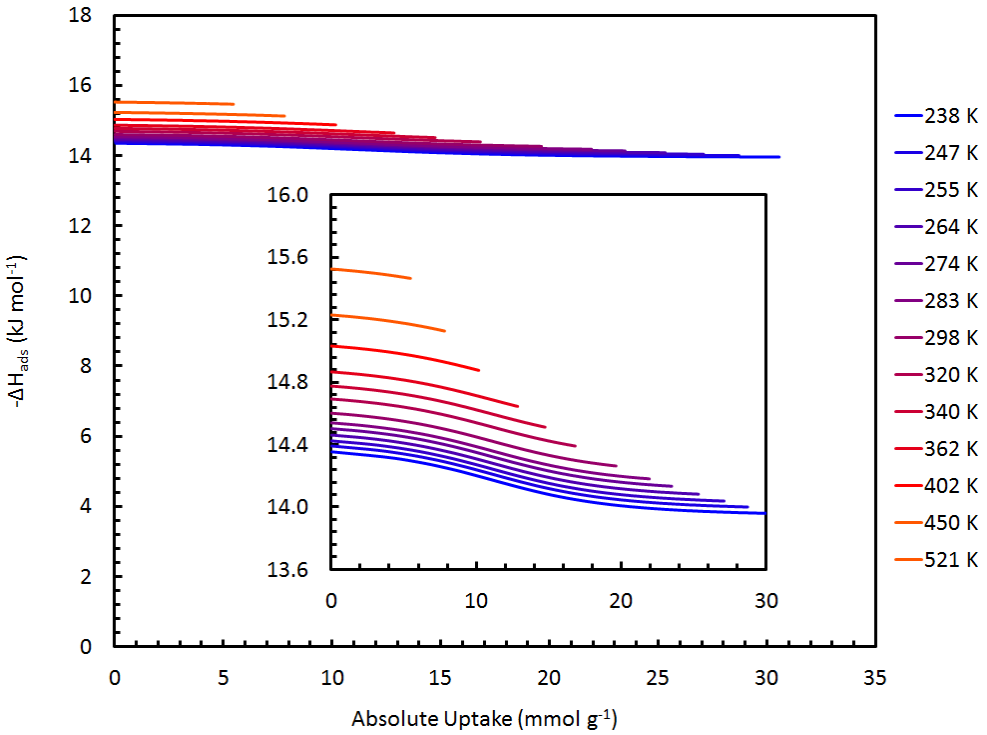

Figure S7. Isosteric enthalpy of adsorption (from Eq. 7), using a double-Langmuir fit with the most commonly implemented ideal gas assumption.

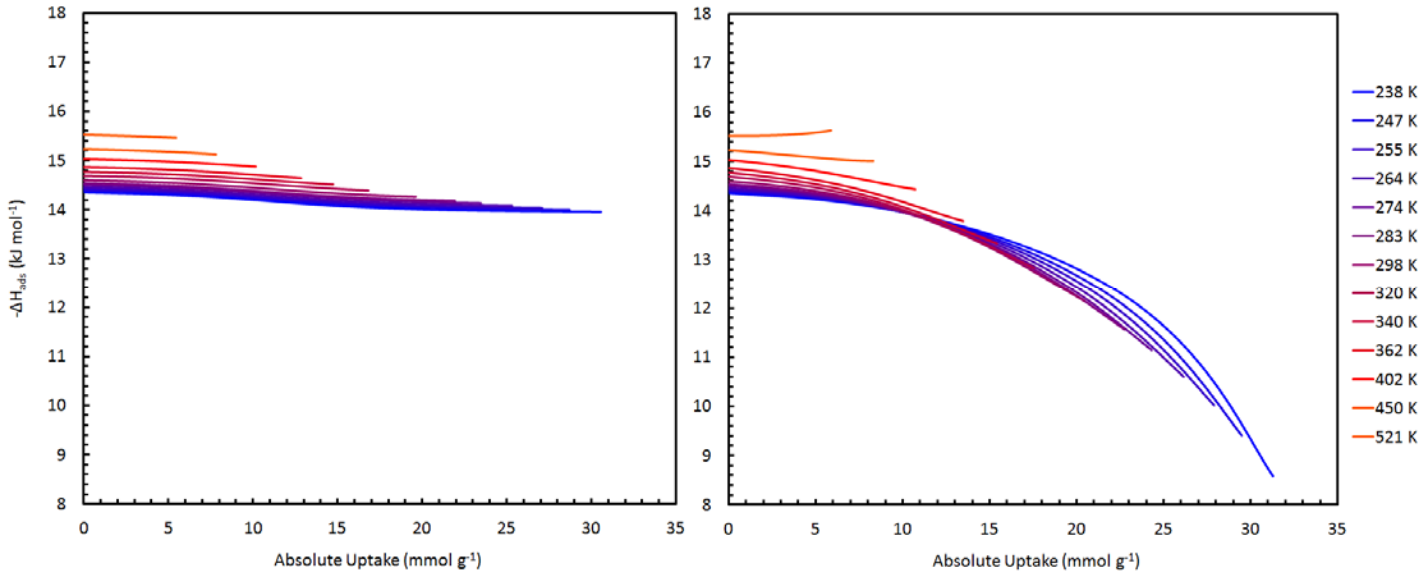

Figure S8. Isosteric enthalpy of adsorption, using double-Langmuir fits: (left) with the ideal gas assumption (Eq. 7), and (right) with the real gas density (Eq. 6), both employing the typical molar volume assumption.

When the real gas data is used, the calculation of isosteric enthalpy changes significantly at high pressures (see Figure S8). Non-ideality of methane in the gas phase is substantial under these conditions and must be taken into account for the most accurate description of adsorption thermodynamics. The tendency of the isosteric heat to a constant value at high uptake[25] is commonly reported as evidence of proper calculation procedures[1, 2]; however this was not observed when ideal gas assumptions were omitted from the calculations in this study. We suggest that a general exception be made for adsorption in the significantly non-ideal gas regime where there is no reason that the isosteric enthalpy of adsorption would persist to a plateau value.

Secondly, the change in molar volume on adsorption must also be carefully considered at high pressure, where the molar volume in the gas phase approaches that of liquid methane. The usual approximation, treating the adsorbed phase volume as negligible compared to that of the gas phase, holds in the low pressure limit, but becomes invalid beyond 1 MPa where the difference in isosteric heat calculated with or without the approximation is >1%, as shown in Figure S9. To approximate the molar volume of the adsorbed phase, we suggest to use that of liquid methane, a value that can be easily determined and which is seen as a reasonable approximation in numerous gas-solid adsorption systems. Specifically, we use $v_a = v_{liq} = 38$ mL mol^{-1}, the value for pure methane at 111.5 K and 0.1 MPa, as shown in Eq. 5. In this case, the difference between the molar volume of the gas and the adsorbed phases becomes significant at all temperatures in this study since v_a is 5-30% the magnitude of v_g at 10 MPa. The variation of the liquid molar volume with temperature and pressure was ~20% of that change, and so was considered to be a negligible complication within the error of the proposed assumption, and a fixed molar volume of the adsorbed phase was used throughout all temperatures and pressures. The resulting calculation of isosteric enthalpy is shown for all three materials in Figure S10.

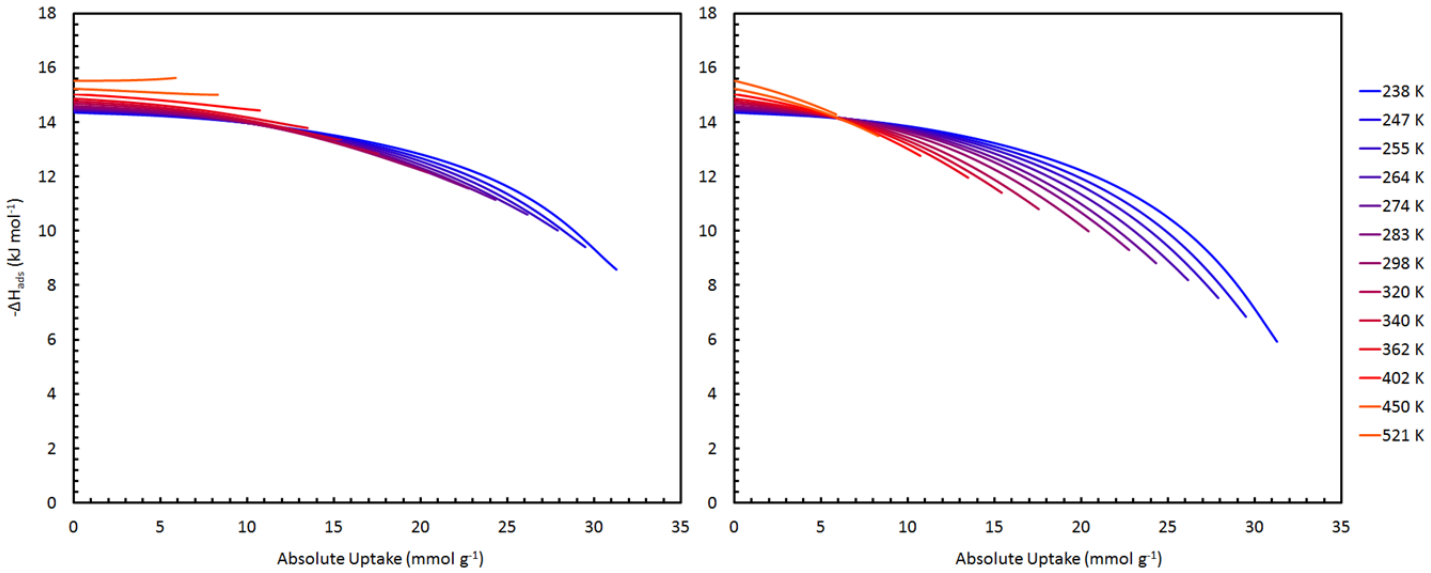

Figure S9. Isosteric enthalpy of adsorption, using double-Langmuir fits: (left) with the common molar volume assumption (Eq. 6), and (right) using a finite adsorbed phase molar volume equal to that of liquid methane (Eq. 5), both using real gas density in the bulk gas phase.

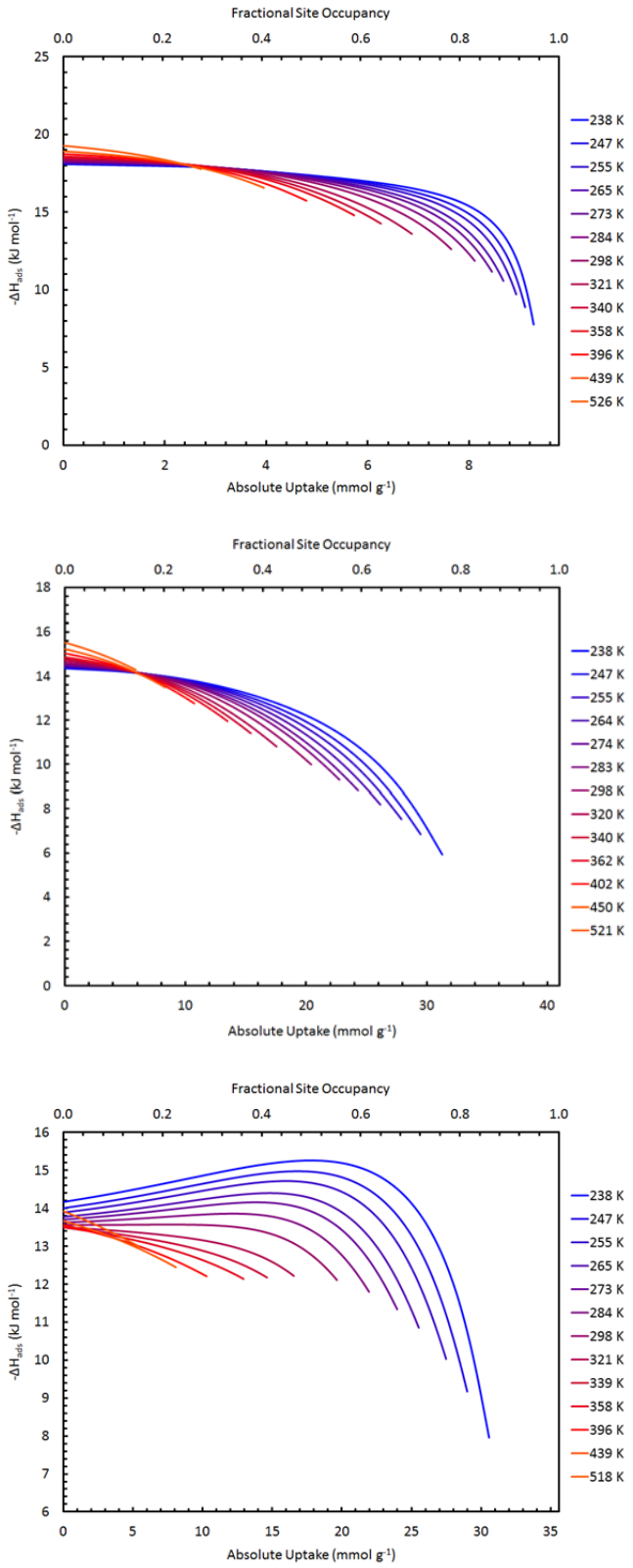

Figure S10. The isosteric heat of adsorption of methane on CNS-201 (top), MSC-30 (middle), and ZTC-3 (bottom), using Eq. 5, taking into account non-ideality of the gas and a finite adsorbed phase volume.

In summary, the method used to determine the pressure dependence of the enthalpy of adsorption of methane on MSC-30 had a significant effect on the results. In every case utilizing the excess adsorption data, the enthalpy diverged at high uptake where the isoexcess assumption is not valid. A double-Langmuir-type equation derived from the definition of Gibbs surface excess was a satisfactory fitting equation in both the model-independent case, and also when used to determine the absolute quantity of adsorption in the isosteric analysis. In the latter case, the enthalpy of adsorption showed reasonable characteristics and conformed to our physical understanding of adsorption at all pressures and temperatures measured. It also gave a Henry's law value closest to that for a model-free analysis of the low pressure data. All simplifying approximations within the derivation of the isosteric enthalpy of adsorption were found to be extremely limited in validity for methane adsorption within the pressure and temperature range of study. Therefore, real gas equation of state data was used and a simple, effective approximation of the finite molar volume of the adsorbed phase was proposed.

VII. Dependence of Optimized Parameters on Surface Area

The optimized fit parameters from the double-Langmuir equation for all three materials were compared to their BET surface area (Figure S11) as calculated from N_2 adsorption at 77 K. As expected, the scaling parameter n_{max} showed a linear trend with BET surface area, in addition to the maximum adsorption volume V_{max}.

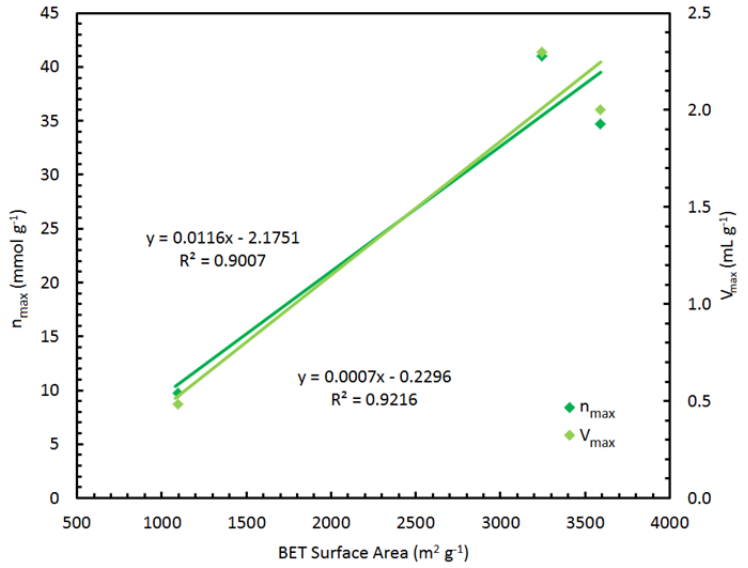

Figure S11. The dependence of fit parameters n_{max} and V_{max} on BET surface area for CNS-201, MSC-30, and ZTC-3.

VIII. Dependence of Measured Uptake Capacity on Surface Area

A well-known rule of thumb for *hydrogen* storage in physisorbent materials is "Chahine's rule"[26] which predicts 1 wt% Gibbs excess maximum uptake per 500 $m^2 g^{-1}$ of BET surface area at 77 K. A similar trend has been shown for methane uptake in physisorbent materials at 298 K,[27, 28] and the carbons in this study are consistent with previous reports (shown in Figure S12). The relationship for methane is 4.4 mmol g^{-1} (6.6 wt%) Gibbs excess maximum uptake per 1000 $m^2 g^{-1}$ of BET surface area at 298 K.

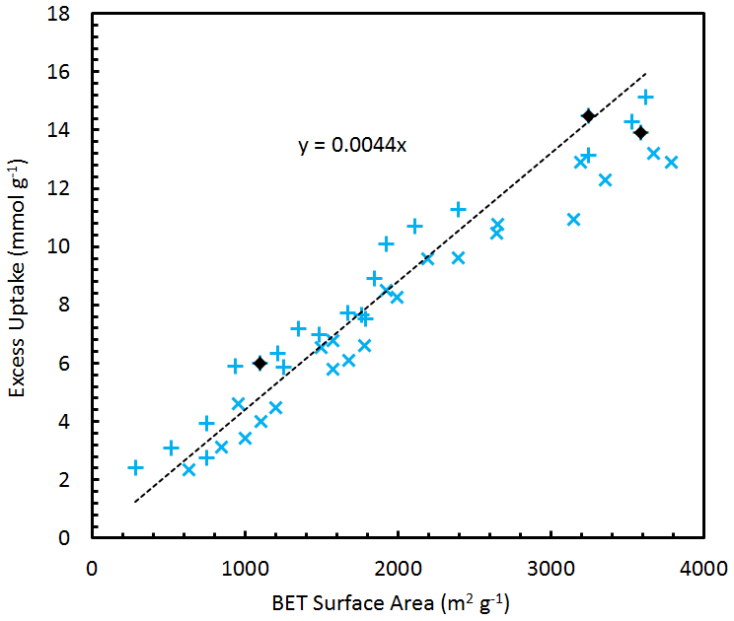

Figure S12. Equilibrium excess adsorption uptake of methane as a function of BET surface area, reported as the excess maximum at 298 K for CNS-201, MSC-30, and ZTC-3 (black diamonds). A + indicates a reported value from the literature.[27] A × indicates a reported value of the BET monolayer capacity from the literature.[28]

IX. Volumetric Storage Capacity

Using the equilibrium excess uptake quantities and the bulk and skeletal densities of the materials studied, summarized in Table 1, the deliverable gravimetric capacity for each material can be determined for a model storage system. The bulk density values are not optimized by any means, and potential for improvement is highest for ZTC-3 (due to its extremely low bulk density) which proved to be the most difficult material to pack by simple means. The bulk densities are therefore a lower bound and are used for approximate comparison purposes only.

The gravimetric deliverable capacity of methane from a 70 L storage vessel weighing 77 kg is shown in Figure S13 for all three materials compared to that from pure gas compression at 238 K. The deliverable amount is taken to be the difference between the amount in the tank at the pressure plotted and that at the "empty" pressure, which is a finite pressure determined by the desired application. For combustion, the empty pressure is expected to be low, but for delivery to a fuel cell, the gaseous fuel must be delivered at pressures above 0.3 MPa which is the value used in Figure S13.

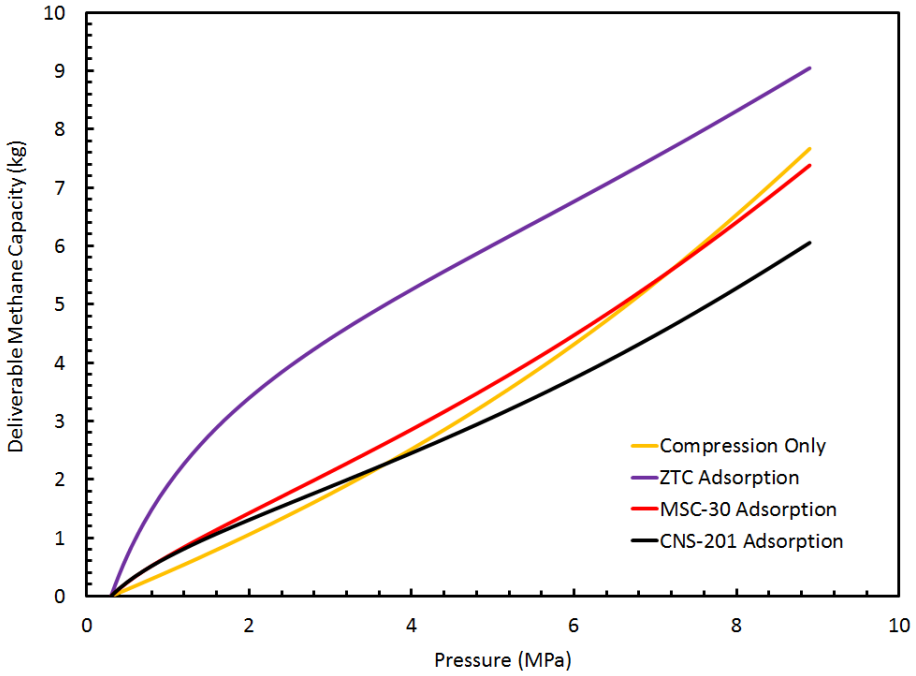

Figure S13. The calculated deliverable quantity of methane gas from a 70 L storage vessel containing no adsorbent (pure gas compression only), compared to that for an adsorbent based storage system of the same size, at 238 K.

The increasing isosteric heat of adsorption on ZTC-3 in the range of pressure associated with methane delivery (>0.3 MPa) is seen to have a dramatic effect on the deliverable quantity stored in a fixed volume of a fixed system mass. If cycled between 0.3-9 MPa, the deliverable storage capacity of a 70 L tank containing ZTC-3 is 20% greater than that for pure compression, and 25% greater than that for a tank containing MSC-30. By improving the compaction of ZTC-3, this figure would increase. Cycling between 0.3-5 MPa, the improvement of a tank containing ZTC-3 over pure compression is 80%.

X. Data Tables

The equilibrium methane adsorption data collected in this study represents one of the largest data sets of high pressure adsorption on carbon materials, and is of value for testing theoretical models of excess and absolute adsorption in the supercritical regime. The following are the experimentally collected isotherm data at all thirteen temperatures (for MSC-30 and ZTC-3) and six temperatures (for CNS-201).

All quantities of uptake are excess adsorption (in mmol g^{-1}) and pressure is given in MPa.

Table 4: Equilibrium excess uptake (n_e) of methane on CNS-201 between 0-9 MPa and 247-526 K.

247 K		255 K		273 K		298 K		340 K	
P	n_e	P	n_e	P	n_e	P	n_e	P	n_e
0.03152	1.67257	0.04229	1.64637	0.05228	1.27878	0.06334	0.91254	0.07967	0.5274
0.07239	2.5821	0.08481	2.43702	0.10549	1.92069	0.13445	1.4835	0.16547	0.91903
0.13591	3.37671	0.15681	3.15692	0.16653	2.44753	0.1796	1.7654	0.19926	1.05814
0.36776	4.85045	0.38306	4.46709	0.39171	3.60815	0.40425	2.71515	0.42178	1.72127
0.34336	4.82206	0.35991	4.47964	0.38473	3.61107	0.43023	2.83989	0.45299	1.83435
0.65027	5.67962	0.65664	5.26539	0.66169	4.38914	0.67356	3.41782	0.67962	2.2663
0.93424	6.16763	0.93808	5.76141	0.93794	4.89898	0.94514	3.89866	0.95054	2.69296
1.30435	6.56888	0.95561	5.92503	1.30697	5.34975	0.98043	4.03178	0.99905	2.81603
0.92459	6.26662	2.00844	6.83832	0.95148	4.97657	1.31377	4.36175	1.31544	3.12939
2.05602	7.17087	3.37154	7.23226	1.70387	5.6841	1.71307	4.71663	1.70861	3.48582
3.37154	7.4546	4.83805	7.23898	2.07256	6.00209	2.09945	5.09704	2.10884	3.77314
4.72222	7.44093	6.1453	7.0695	3.38808	6.41418	3.44393	5.67153	2.10566	3.81896
6.09772	7.19462	7.4753	6.83372	4.78841	6.60544	4.81323	5.91865	2.61693	4.0482
7.45047	6.80867	8.79495	6.52202	6.14323	6.55984	6.16598	5.98388	3.14155	4.27859
8.86735	6.32538			7.52701	6.43028	7.58596	5.92181	3.42325	4.47431
				8.88803	6.23452	8.98008	5.85881	4.80909	4.81467
								6.17219	5.06671
								7.56631	5.12316
								8.99352	5.16602

526 K	
P	n_e
0.097819	0.069506
0.19719	0.112226
0.226741	0.152351
0.452856	0.288719
0.501249	0.277787
0.708568	0.430165
0.97468	0.563666
1.05145	0.551184
1.338117	0.719586
1.730618	0.867242
2.126852	1.004889
2.160127	1.019048
2.623078	1.175894
3.149701	1.334875
3.448758	1.390724
4.840809	1.719674
6.191492	1.972601
7.544243	2.147271
8.923884	2.320326

Table 5. Equilibrium excess uptake (n_e) of methane on MSC-30 between 0-9 MPa and 238-521 K. Excess uptake is in units of mmol g^{-1}, and pressure is in MPa.

238 K		247 K		255 K		264 K		274 K	
P	n_e	P	n_e	P	n_e	P	n_e	P	n_e
0.05833	2.9238	0.06403	2.45831	0.06851	2.11609	0.07259	1.78676	0.07857	1.53347
0.11997	4.69747	0.13031	4.10954	0.13858	3.6424	0.14893	3.16232	0.15306	2.57795
0.16659	5.99416	0.17429	5.02072	0.18157	4.34218	0.19018	3.7357	0.19962	3.20815
0.38337	9.58601	0.39147	8.2111	0.40169	7.2246	0.40603	6.23223	0.41481	5.37494
0.38886	9.60792	0.40127	8.44362	0.41162	7.38545	0.42403	6.45678	0.42816	5.57936
0.64855	12.1436	0.65332	10.6203	0.6606	9.45941	0.66548	8.29874	0.67052	7.241
0.92612	13.9381	0.92823	12.3509	0.94684	11.1896	0.93906	9.90769	0.93956	8.71834
1.29423	15.5909	1.2942	13.9885	1.30041	12.7407	1.30609	11.5053	1.31153	10.254
0.93286	14.1493	0.94734	12.7338	0.94734	11.3984	0.96389	10.2582	0.95975	8.96193
1.68779	16.9261	1.6907	15.3031	1.69771	14.0657	1.69753	12.7683	1.6995	11.4799
2.02292	18.2268	2.03533	16.5959	2.03533	15.1829	2.05188	13.9954	2.04981	12.6185
3.31569	20.6412	3.3343	18.8821	3.33637	17.6298	3.34672	16.3614	3.35292	14.8886
4.6643	21.6807	4.68499	19.9797	4.69947	18.9025	4.70153	17.8168	4.71188	16.1946
6.0274	21.6092	6.05842	20.1924	6.0667	19.4372	6.08738	18.4286	6.106	16.9328
7.39049	20.4545	7.41945	19.8207	7.44427	19.2498	7.50012	18.4075	7.47943	17.1863
8.76599	18.7465	8.78875	18.8379	8.77634	18.6868	8.85287	17.978	8.8508	16.9893

283 K		298 K		320 K		340 K		362 K	
P	n_e	P	n_e	P	n_e	P	n_e	P	n_e
0.08102	1.26426	0.08583	0.99576	0.08681	0.72106	0.09239	0.54439	0.094979	0.430147
0.16547	2.36311	0.17582	1.90399	0.1903	1.50583	0.19857	1.06281	0.196501	0.875872
0.20274	2.70332	0.20382	2.0854	0.20706	1.55225	0.21438	1.19026	0.214036	0.909031
0.33033	3.89333	0.42207	3.66646	0.43104	2.82131	0.4361	2.20365	0.439484	1.723959
0.44471	4.95187	0.45712	4.06506	0.48194	3.14552	0.49022	2.38996	0.490217	1.849482
0.47045	4.99361	0.67952	5.12491	0.68889	4.01374	0.69328	3.19194	0.697329	2.53159
0.69177	6.40959	0.94723	6.33031	0.95273	5.02437	0.95659	4.06614	0.960241	3.260971
0.94548	7.68997	0.99698	6.66047	1.32764	6.212	1.31962	5.08994	1.322611	4.131244
0.9825	8.07819	1.32053	7.66942	1.01973	5.36591	1.03421	4.22971	1.034214	3.515799
1.30932	9.12433	1.70637	8.76495	1.70974	7.21361	1.71626	6.02772	1.715512	4.943074
1.70035	10.3131	2.08497	9.83784	2.10773	8.19921	2.12221	6.78673	2.128412	5.737387
2.06739	11.4622	3.37981	12.0743	3.40256	10.3124	3.42532	8.76072	3.410836	7.611534
3.36533	13.7431	4.74084	13.3635	4.77186	11.6409	4.78014	10.1134	4.765656	8.982563
4.72842	15.0664	6.11634	14.1824	6.14323	12.5508	6.14943	11.1424	6.145297	10.07682
6.11634	15.7619	7.49598	14.4775	7.52494	13.2593	7.52494	11.8791	7.518733	10.61905
7.48564	16.0976	8.91492	14.4206	8.8901	13.6037	8.91078	12.2573	8.867347	11.06398
8.85287	15.9519								

402 K		450 K		521 K	
P	n_e	P	n_e	P	n_e
0.095312	0.264322	0.206843	0.312932	0.100032	0.096919
0.21098	0.516237	0.504696	0.802983	0.208911	0.257445
0.219435	0.577949	1.056966	1.547822	0.223222	0.202398
0.44715	1.100658	2.161506	2.802391	0.457736	0.419764
0.500559	1.168727	3.456342	4.001805	0.506765	0.563646
0.707795	1.645824	4.811162	4.905019	0.710382	0.622786
0.966574	2.132081	6.199076	5.49889	0.97396	0.810212
1.328544	2.775085	7.599401	6.312641	1.345529	1.092771
1.048693	2.319473	8.962495	6.740001	1.06524	1.107253
1.716512	3.365324			1.732164	1.375554
2.142891	3.947574			2.175985	1.892646
3.435658	5.410322			3.468752	2.647447
4.804956	6.461805			4.827709	3.077738
6.170118	7.287202			6.188734	3.767925
7.560101	7.917329			7.589059	4.672123
8.925263	8.275128			8.958358	5.060649

Table 6. Equilibrium excess uptake (n_e) of methane on ZTC-3 between 0-9 MPa and 238-518 K.

238 K		247 K		255 K		265 K		273 K	
P	n_e	P	n_e	P	n_e	P	n_e	P	n_e
0.08851	2.74035	0.08679	2.13278	0.08785	1.7617	0.08958	1.3912	0.09042	1.19214
0.16961	4.59656	0.17168	3.77235	0.18202	3.26497	0.18616	2.77652	0.18823	2.0028
0.2029	5.27133	0.20612	4.2689	0.20957	3.63528	0.21157	2.90978	0.21121	2.51615
0.42155	8.91232	0.4269	7.35128	0.43062	6.29889	0.43635	5.16111	0.43412	4.5226
0.45092	9.40485	0.45505	7.93782	0.46333	6.73821	0.46953	5.71611	0.47574	4.58662
0.6774	11.9303	0.68328	9.99992	0.68526	8.70216	0.6898	7.23912	0.69237	6.41887
0.94884	14.2414	0.95019	12.0991	0.95218	10.6767	0.95497	8.99989	0.95595	8.03245
1.32374	16.4732	1.31149	14.1354	1.31361	12.7497	1.31735	10.9502	1.31765	9.80274
0.99078	14.992	0.97837	12.7874	1.00319	11.2714	1.0156	9.66277	1.01767	8.04942
1.70425	18.0077	1.71079	15.7958	1.70465	14.3496	1.70998	12.5064	1.70749	11.3014
2.06843	19.806	2.06843	17.5107	2.08291	15.9724	2.13255	14.2609	2.10359	12.1293
3.34465	21.9819	3.35499	19.719	3.35085	18.615	3.42945	16.8004	3.43359	14.7722
4.68085	22.1343	4.69533	20.5004	4.70153	19.7399	4.7429	17.9216	4.74704	16.2179
6.04188	21.4464	6.05015	20.2592	6.06877	20.2461	6.09359	18.5297	6.10393	16.9999
7.37394	19.9073	7.4029	19.6406	7.41945	19.7629	7.45668	18.1864	7.4753	16.9993
8.70394	18.2061	8.74945	18.8376	8.78461	18.8635	8.81977	17.7636	8.83218	16.6217

284 K		298 K		321 K		339 K		358 K	
P	n_e	P	n_e	P	n_e	P	n_e	P	n_e
0.09123	0.88433	0.093912	0.767091	0.0953	0.54893	0.10247	0.43382	0.096459	0.323046
0.1965	2.06013	0.198569	1.525807	0.20271	1.18196	0.20684	0.88951	0.21098	0.78299
0.21736	2.00538	0.216702	1.623577	0.21582	1.15255	0.22593	0.92303	0.218849	0.698188
0.44294	3.68469	0.441884	2.959302	0.4386	2.14771	0.44498	1.72043	0.445363	1.315477
0.50056	4.35259	0.494354	3.082729	0.49642	2.38748	0.52331	1.91015	0.506765	1.647565
0.69745	5.27895	0.696663	4.262035	0.69725	3.17345	0.69882	2.54886	0.700142	1.953702
0.96076	6.70279	0.961174	5.421924	0.96203	4.09233	0.9732	3.35164	0.97132	2.576551
1.04042	7.4082	1.036282	5.813822	1.0549	4.28315	1.05697	3.56373	1.054898	2.89235
1.32366	8.28589	1.323678	6.789015	1.32066	5.19525	1.32517	4.27993	1.33449	3.339732
1.72003	9.6975	1.713379	7.996622	1.71103	6.26021	1.71527	5.17057	1.721525	4.032177
2.12014	11.1833	2.126343	9.241572	2.10913	7.19584	2.11204	5.97504	2.116959	4.708681
3.40463	13.8392	3.412905	11.66409	2.12841	7.11606	2.14496	6.00636	2.153233	4.899497
4.75531	15.3532	4.753246	12.94425	2.60936	8.20323	2.61	6.90677	2.614118	5.477988
6.12875	16.0017	6.124613	13.83233	3.13225	9.16678	3.14116	7.77021	3.143808	6.124452
7.53114	16.1515	7.506322	14.0912	3.4129	9.30043	3.43359	8.0335	3.441863	6.760846
8.88389	15.6163	8.869416	13.75196	4.73877	10.8634	4.78634	9.4703	4.794614	7.933946
0.09123	0.88433	0.093912	0.767091	6.11427	11.9473	6.15771	10.5049	6.159776	9.011308
				7.55803	12.6389	7.51873	11.2003	7.529075	9.661693
				8.89631	12.9869	8.98525	11.7674	8.914921	9.868008

396 K		439 K		518 K	
P	n_e	P	n_e	P	n_e
0.098045	0.220005	0.100858	0.120166	0.102765	0.079153
0.221102	0.467406	0.223382	0.27326	0.22339	0.061015
0.22339	0.461032	0.235801	0.281368	0.225821	0.164918
0.450016	0.903976	0.455363	0.547338	0.454869	0.336001
0.523312	0.943054	0.533654	0.709964	0.531586	0.291516
0.705995	1.367028	0.713208	0.829307	0.711581	0.530536
0.998505	1.849129	0.979053	1.119177	0.977226	0.727606
1.075582	1.916965	1.100403	1.398448	1.094198	0.657902
1.341676	2.362146	1.340223	1.504728	1.342663	0.953889
1.726711	2.926605	1.730591	1.875245	1.733964	1.207439
2.122545	3.443224	2.126825	2.263501	2.15193	1.415868
2.186328	3.473505	2.20908	2.44604	2.211149	1.343479
2.623971	4.042535	2.63105	2.705292	2.63669	1.697484
3.152194	4.616633	3.154074	3.219059	3.232508	2.017694
3.470821	4.831019	4.19477	3.866671	3.503916	2.077024
4.815298	6.115046	5.082126	4.5686	4.893899	2.84219
6.186666	7.102554	6.283882	5.230203	6.306634	3.552917
7.591128	7.807846	7.61388	5.890184	7.665591	4.243635
8.943879	8.214734	9.024548	6.265714	9.086601	4.682551

XI. Supporting Information References

(1) F. O. Mertens, 'Determination of absolute adsorption in highly ordered porous media', *Surf. Sci.,* **603**, 1979-84 (2009).

(2) R. J. Olsen, 'Investigations of novel hydrogen adsorption phenomena', thesis, University of Missouri (2011).

(3) A. L. Myers, J. A. Calles, and G. Calleja, 'Comparison of molecular simulation of adsorption with experiment', *Adsorption,* **3**, 107-15 (1997).

(4) N. P. Stadie, J. J. Vajo, R. W. Cumberland, A. A. Wilson, C. C. Ahn, and B. Fultz, 'Zeolite-templated carbon materials for high-pressure hydrogen storage', *Langmuir,* **28**, 10057-63 (2012).

(5) H. Nishihara, P. X. Hou, L. X. Li, M. Ito, M. Uchiyama, T. Kaburagi, A. Ikura, J. Katamura, T. Kawarada, K. Mizuuchi, and T. Kyotani, 'High-pressure hydrogen storage in zeolite-templated carbon', *J. Phys. Chem. C,* **113**, 3189-96 (2009).

(6) Z. Yang, Y. Xia, and R. Mokaya, 'Enhanced hydrogen storage capacity of high surface area zeolite-like carbon materials', *J. Am. Chem. Soc.,* **129**, 1673-79 (2007).

(7) J. B. Dumas, 'A method of estimating nitrogen in organic material', *Ann. Chim. et Phys.,* **58**, 171 (1833).

(8) P. Tarazona, U. M. B. Marconi, and R. Evans, 'Phase equilibria of fluid interfaces and confined fluids', *Mol. Phys.,* **60**, 573-95 (1987).

(9) J. J. Purewal, H. Kabbour, J. J. Vajo, C. C. Ahn, and B. Fultz, 'Pore size distribution and supercritical hydrogen adsorption in activated carbon fibers', *Nanotechnology,* **20**, 204012 (2009).

(10) T. Voskuilen, T. Pourpoint, and A. Dailly, 'Hydrogen adsorption on microporous materials at ambient temperatures and pressures up to 50 MPa', *Adsorption,* **18**, 239-49 (2012).

(11) K. R. Matranga, A. L. Myers, and E. D. Glandt, 'Storage of natural gas by adsorption on activated carbon', *Chem. Eng. Sci.,* **47**, 1569-79 (1992).
(12) D. Nicholson, 'Simulation studies of methane transport in model graphite micropores', *Carbon,* **36**, 1511-23 (1998).
(13) T. P. McNicholas, A. Wang, K. O'Neill, R. J. Anderson, N. P. Stadie, A. Kleinhammes, P. Parilla, L. Simpson, C. C. Ahn, Y. Wang, Y. Wu, and J. Liu, 'H2 storage in microporous carbons from PEEK precursors', *J. Phys. Chem. C,* **114**, 13902-08 (2010).
(14) N. P. Stadie, J. J. Purewal, C. C. Ahn, and B. Fultz, 'Measurements of hydrogen spillover in platinum doped superactivated carbon', *Langmuir,* **26**, 15481-85 (2010).
(15) T. Kiyobayashi, H. T. Takeshita, H. Tanaka, N. Takeichi, A. Züttel, L. Schlapbach, and N. Kuriyama, 'Hydrogen adsorption in carbonaceous materials – how to determine the storage capacity accurately', *J. Alloys Compd.,* **330-332**, 666-69 (2002).
(16) E. W. Lemmon, M. L. Huber, and M. O. McLinden, 'NIST standard reference database 23: reference fluid thermodynamic and transport properties − REFPROP', Number Version 8.0 in Standard Reference Data Program (2007).
(17) N. P. Stadie, 'Synthesis and thermodynamic studies of physisorptive energy storage materials', thesis, California Institute of Technology (2012).
(18) J. Purewal, D. Liu, A. Sudik, M. Veenstra, J. Yang, S. Maurer, U. Müller, and D. J. Siegel, 'Improved hydrogen storage and thermal conductivity in high-density MOF-5 composites', *J. Phys. Chem. C,* **116**, 20199-212 (2012).
(19) S. Sircar, 'Gibbsian surface excess for gas adsorption – revisited', *Ind. Eng. Chem. Res.,* **38**, 3670-82 (1999).
(20) G. Aranovich and M. Donohue, 'Determining surface areas from linear adsorption isotherms at supercritical conditions', *J. Colloid Interface Sci.,* **194**, 392-97 (1997).
(21) D. Saha, Z. Wei, and S. Deng, 'Equilibrium, kinetics, and enthalpy of hydrogen adsorption in MOF-177', *Int. J. Hydrogen Energy,* **33**, 7479-88 (2008).
(22) S. Ono and S. Kondo, *Molecular theory of surface tension in liquids*, Springer-Verlag, Berlin (1960).
(23) G. L. Aranovich and M. D. Donohue, 'Adsorption isotherms for microporous adsorbents', *Carbon,* **33**, 1369-75 (1995).
(24) C. Kittel, *Thermal physics*, John Wiley, New York (1969).
(25) A. Chakraborty, B. B. Saha, S. Koyama, K. C. Ng, and S.-H. Yoon, 'Thermodynamic trends in the uptake capacity of porous adsorbents on methane and hydrogen', *Appl. Phys. Lett.,* **92**, 201911-3 (2008).
(26) E. Poirier, R. Chahine, and T. K. Bose, 'Hydrogen adsorption in carbon nanostructures', *Int. J. Hydrogen Energ.,* **26**, 831-35 (2001).
(27) Y. Sun, C. Liu, W. Su, Y. Zhou, and L. Zhou, 'Principles of methane adsorption and natural gas storage', *Adsorption,* **15**, 133-37 (2009).
(28) J. Alcañiz-Monge, D. Lozano-Castelló, D. Cazorla-Amorós, and A. Linares-Solano, 'Fundamentals of methane adsorption in microporous carbons', *Microporous Mesoporous Mater.,* **124**, 110-16 (2009).